Available online at www.sciencedirect.com
SCIENCE DIRECT®
Journal of Sound and Vibration 274 (2004) 1045–1063
JOURNAL OF SOUND AND VIBRATION
www.elsevier.com/locate/jsvi

Identification of vehicles moving on continuous bridges with rough surface

R.J. Jiang, F.T.K. Au*, Y.K. Cheung

Department of Civil Engineering, The University of Hong Kong, Pokfulam Road, Hong Kong, People's Republic of China

Received 28 January 2003; accepted 23 May 2003

Abstract

This paper describes the parameter identification of vehicles moving on multi-span continuous bridges taking into account the surface roughness. Each moving vehicle is modelled as a two-degree-of-freedom system that comprises five components: a lower mass and an upper mass, which are connected together by a damper and a spring, together with another spring to represent the contact stiffness between the tyres and the bridge deck. The corresponding parameters of these five components, namely, the equivalent values of the two masses, the damping coefficient, and the two spring stiffnesses together with the roughness parameters are identified based on dynamic simulation of the vehicle–bridge system. In the study, the accelerations at selected measurement stations are simulated from the dynamic analysis of a continuous beam under moving vehicles taking into account randomly generated bridge surface roughness, together with the addition of artificially generated measurement noise. The identification is realized through a robust multi-stage optimization scheme based on genetic algorithms, which searches for the best estimates of parameters by minimizing the errors between the measured accelerations and the reconstructed accelerations from the identified parameters. Starting from the very wide initial variable domains, this multi-stage optimization scheme reduces the variable search domains stage by stage using the identified results of the previous stage. A few test cases are carried out to verify the efficiency of the multi-stage optimization procedure. The identified parameters are also used to estimate the time-varying contact forces between the vehicles and the bridge.

1. Introduction

Vehicle parameter identification has been studied for various purposes, such as the prediction and analysis of the dynamic responses of the vehicles and bridges, and various design aspects

*Corresponding author. Tel.: +852-2859-2650; fax: +852-2559-5337.
E-mail address: francis.au@hku.hk (F.T.K. Au).

0022-460X/$ - see front matter
doi:10.1016/S0022-460X(03)00664-3

including the riding quality, structure-borne noise, the impact loading on the bridges and so on. The dynamic interaction between the vehicle and the bridge depends greatly on their respective dynamic properties represented by their mass distributions, stiffnesses and damping, as well as the contact surface condition between the vehicle and the bridge. The vertical motion of a vehicle running on a bridge is mainly induced by the random road surface roughness [1–4] and the ensuing vibration of the bridge. Also important are the properties of the tyres [5–8], especially the vertical tyre stiffness and the tyre damping [9,10]. For simplicity, the road surface irregularities and the properties of the tyres are seldom considered at the same time, but their interaction often cannot be dismissed as negligible. When the study is focused on the wheel/rail noise [1–4] induced by the contact vibration or the dynamic behaviour [5] of the moving vehicle, road surface roughness and tyre stiffness are often regarded as important and therefore considered together. However when the bridge response is the focus, often only either the road surface roughness [11] or the tyre stiffness [12] is considered. As these factors are inherently uncertain, sometimes neither of these factors is considered [13,14]. In the identification of dynamic loading on bridges, the quantity to predict is the moving force, and hence the road surface irregularities and the tyre stiffness have been implicitly accounted for [15]. In a study of the dynamic loading by highway vehicles [7], the peak dynamic loads caused by highway surface irregularities are as much as twice the static loads, while the tyre stiffness is found to be a critical factor. In view of this, the present study has taken both these factors into account.

For the parameter identification of vehicles running on continuous bridges, the moving mass model [16] and the 4-parameter vehicle model [17] have been studied. To better account for the road surface irregularities and the tyre stiffness, a more sophisticated 5-parameter vehicle model is proposed. Each moving vehicle is modelled as a two-degree-of-freedom (2-d.o.f.) system that comprises five components: a lower mass and an upper mass, which are connected together by a damper and a spring, together with another spring to represent the contact stiffness between the tyres and the bridge deck. The corresponding parameters of these five components, namely, the equivalent values of the two masses, the damping coefficient, and the two spring stiffnesses together with the roughness parameters are identified based on the acceleration measurements at various stations along the continuous bridge. The acceleration measurements are simulated from the dynamic analysis of a continuous bridge under moving vehicles based on the modified beam vibration functions [14] and modal superposition, taking into account the randomly generated bridge road surface roughness together with the addition of artificially generated measurement noise. The identification is carried out through a robust multi-stage optimization scheme [17] based on genetic algorithms [18,19], which searches for the global optimal values of parameters by minimizing the errors between the measured accelerations and the reconstructed accelerations from the identified parameters in each stage. Starting from the very wide initial variable domains, this multi-stage optimization scheme reduces the variable search domains stage by stage based on the identified results of the previous stage. A series of comprehensive case studies are then carried out to verify the validity of the method. The effects of different levels of measurement noise, number of measurement stations, and number of vehicles on the identified results are studied. The time-dependent contact forces between the moving vehicles and the bridge surface are then calculated from the identified parameters. The work described in this paper will be useful to the operation and structural health monitoring of bridges.

2. Simulation of acceleration measurements

2.1. Modelling of vehicles and bridge

In this paper, a multi-span continuous bridge is modelled as a linear elastic Bernoulli–Euler beam with totally $(P+1)$ point supports as shown in Fig. 1. The bridge may have varying sections characterised by the density $\rho(x)$, cross-sectional area $A(x)$, Young's modulus $E(x)$ and moment of inertia $I(x)$ at location x. The N moving vehicles on the bridge are modelled as 2-d.o.f. systems each with five parameters $\{M_{s1}, M_{s2}, c_s, k_{s1}, k_{s2},\ s = 1, 2, \ldots, N\}$. The typical sth moving vehicle is modelled by the lower mass M_{s1} and upper mass M_{s2}, which are interconnected by a primary spring of stiffness k_{s2} and a dashpot of damping coefficient c_s. The tyre contact stiffness is represented by another spring with stiffness k_{s1}. The convoy of vehicles moves from left to right along the bridge at a speed $v(t)$, a function of time t. Setting the position of the leftmost point support of the bridge as the origin O, the horizontal position of the sth vehicle is defined as $x_s(t)$. The deflection of the bridge at position x and at time t is denoted by $y(x,t)$ where upward deflection is taken as positive, as shown in Fig. 1. The vertical displacements of the lower and upper masses of the sth vehicle are respectively represented by $\{y_{s1}(t), y_{s2}(t),\ s = 1, 2, \ldots, N\}$, which are also measured vertically upwards with reference to their respective vertical static equilibrium positions before coming on to the bridge.

If the bridge road surface roughness at location x is denoted by $r(x)$, which is also measured vertically upwards with reference to the deck level, the roughness under the sth vehicle wheel is represented by $r(x_s(t))$. Assuming the vehicle convoy speed $v(t)$ is within such a limit that there is no separation between vehicles and bridge surface, the additional elongation Δ_1 of the lower spring during vehicle motion is then expressed as

$$\Delta_1 = y_{s1}(t) - [y(x_s, t) + r(x_s(t))]. \tag{1}$$

The equations of motion of the masses M_{s1} and M_{s2} are, respectively,

$$M_{s1}\frac{\mathrm{d}^2 y_{s1}(t)}{\mathrm{d}t^2} = -k_{s1}\Delta_1 + k_{s2}[y_{s2}(t) - y_{s1}(t)] + c_s\left[\frac{\mathrm{d}y_{s2}(t)}{\mathrm{d}t} - \frac{\mathrm{d}y_{s1}(t)}{\mathrm{d}t}\right], \tag{2}$$

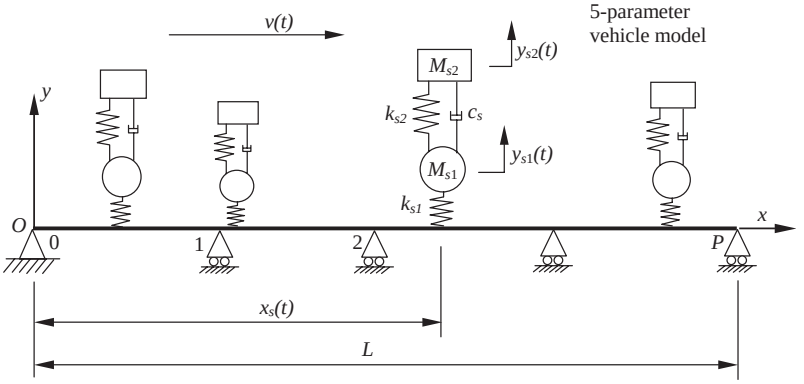

Fig. 1. A multi-span continuous bridge with N moving vehicles.

$$M_{s2}\frac{d^2y_{s2}(t)}{dt^2} = -k_{s2}[y_{s2}(t) - y_{s1}(t)] - c_s\left[\frac{dy_{s2}(t)}{dt} - \frac{dy_{s1}(t)}{dt}\right]. \tag{3}$$

The contact force $f_{cs}(t)$ between the sth vehicle and the bridge can be expressed as

$$f_{cs} = (M_{s1} + M_{s2})g - k_{s1}\Delta_1, \tag{4}$$

where g is the acceleration due to gravity. Eliminating the elongation Δ_1 of the lower spring with Eqs. (2) and (3), Eq. (4) becomes

$$f_{cs} = (M_{s1} + M_{s2})g + M_{s1}\frac{d^2y_{s1}(t)}{dt^2} + M_{s2}\frac{d^2y_{s2}(t)}{dt^2}. \tag{5}$$

By modal superposition and separation of variables, the vibration of the bridge can be expressed as

$$y(x,t) = \sum_{i=1}^{n} q_i(t)\phi_i(x), \tag{6}$$

where $\{q_i(t),\ i = 1, 2, \ldots, n\}$ are the generalized co-ordinates, n is the number of the adopted vibration modes, and $\{\phi_i(x),\ i = 1, 2, \ldots, n\}$ are the assumed vibration modes. For the modelling of the continuous bridge, the modified beam vibration functions [14] are chosen, which are built up from the vibration modes of a hypothetical single-span simply supported beam having the same end supports and total length as the real beam, and cubic spline expressions that ensure the boundary conditions at all the supports. The modified beam vibration functions have been used instead of the conventional mode shapes mainly because of the ease of obtaining them and the ease of subsequent computer programming. Therefore the assumed vibration modes can be written as

$$\phi_i(x) = \bar{\phi}_i(x) + \tilde{\phi}_i(x), \tag{7}$$

where $\{\bar{\phi}_i(x),\ i = 1, 2, \ldots, n\}$ are the first n vibration modes of a hypothetical beam of total length L with the same end supports as the continuous beam but without the intermediate supports, and $\{\tilde{\phi}_i(x),\ i = 1, 2, \ldots, n\}$ are the augmenting cubic spline expressions which are so chosen that each $\phi_i(x)$ satisfies the boundary conditions at the two ends and the zero deflection conditions at the intermediate point supports.

2.2. Simulation of noise-free accelerations considering roughness

Based on the vehicle and bridge models introduced above, dynamic analysis of the system can be carried out and the simulated noise-free acceleration measurements at specified stations of the bridge can be obtained for the subsequent study in parameter identification of the vehicles. The velocity of vibration and the curvature of the beam at position x are, respectively,

$$\frac{\partial y(x,t)}{\partial t} = \sum_{i=1}^{n} \dot{q}_i(t)\phi_i(x), \tag{8}$$

$$\frac{\partial^2 y(x,t)}{\partial x^2} = \sum_{i=1}^{n} q_i(t)\ \phi_i''(x), \tag{9}$$

in which the dot represents differentiation with respect to time t, and the prime represents differentiation with respect to the abscissa x. Therefore the kinetic energy V and the bending energy U are, respectively,

$$V = \frac{1}{2}\int_0^L \rho(x)A(x)\left[\frac{\partial y(x,t)}{\partial t}\right]^2 \mathrm{d}x = \frac{1}{2}\sum_{i=1}^{n}\sum_{j=1}^{n}\dot{q}_i(t)m_{ij}\dot{q}_j(t), \tag{10}$$

$$U = \frac{1}{2}\int_0^L E(x)I(x)\left[\frac{\partial^2 y(x,t)}{\partial x^2}\right]^2 \mathrm{d}x = \frac{1}{2}\sum_{i=1}^{n}\sum_{j=1}^{n}q_i(t)k_{ij}q_j(t), \tag{11}$$

where m_{ij} and k_{ij} are, respectively, the generalized mass and stiffness matrices of the bridge, which can be written as

$$m_{ij} = \int_0^L \rho(x)\,A(x)\phi_i(x)\phi_j(x)\,\mathrm{d}x, \tag{12}$$

$$k_{ij} = \int_0^L E(x)I(x)\phi_i''(x)\phi_j''(x)\,\mathrm{d}x. \tag{13}$$

The generalized force $F_{is}(t)$ corresponding to the contact force $f_{cs}(t)$ can be expressed as

$$F_{is}(t) = -f_{cs}(t)\phi_i(x_s(t)). \tag{14}$$

From Eqs. (5) and (14), $F_{is}(t)$ can be further written as

$$F_{is}(t) = -(M_{s1}+M_{s2})g\phi_i(x_s(t)) - M_{s1}\ddot{y}_{s1}(t)\phi_i(x_s(t)) - M_{s2}\ddot{y}_{s2}(t)\phi_i(x_s(t)). \tag{15}$$

The Lagrangian equation of the bridge is written in terms of the Lagrangian function $\Gamma = V - U$ and the generalized force $F_i(t)$ as

$$\frac{\mathrm{d}}{\mathrm{d}t}\left(\frac{\partial \Gamma}{\partial \dot{q}_i}\right) - \frac{\partial \Gamma}{\partial q_i} = F_i(t), \quad i = 1, 2, \ldots, n, \tag{16}$$

where the generalized force $F_i(t)$ can be written as

$$F_i(t) = \sum_{s=1}^{N} F_{is}(t). \tag{17}$$

Substituting Eqs. (10), (11), (15) and (17) into Eq. (16) and rearranging results in

$$\sum_{j=1}^{n} m_{ij}\ddot{q}_j(t) + \sum_{j=1}^{n} k_{ij}q_j(t) + \sum_{s=1}^{N} M_{s1}\phi_i(x_s(t))\ddot{y}_{s1}(t) + \sum_{s=1}^{N} M_{s2}\phi_i(x_s(t))\ddot{y}_{s2}(t) = p_i(t),$$
$$i = 1, 2, \ldots, n, \tag{18}$$

where

$$p_i(t) = -\sum_{s=1}^{N}(M_{s1}+M_{s2})g\phi_i(x_s(t)). \tag{19}$$

Should a particular vehicle be outside the bridge, the corresponding terms under the summation signs should be omitted.

On the other hand, substituting Eqs. (1) and (6) into Eq. (2) and rearranging, one obtains the equation of motion of M_{s1} as

$$-\sum_{j=1}^{n} k_{s1}\phi_j(x_s(t))q_j + M_{s1}\ddot{y}_{s1}(t) + c_s\dot{y}_{s1}(t) + (k_{s1}+k_{s2})y_{s1}(t) - c_s\dot{y}_{s2}(t) - k_{s2}y_{s2}(t) = k_{s1}r(x_s(t)),$$
$$s = 1, 2, \ldots, N. \tag{20}$$

Likewise the equation of motion of M_{s2} as shown in Eq. (3) can be rewritten as

$$-c_s\dot{y}_{s1}(t) - k_{s2}y_{s1}(t) + M_{s2}\ddot{y}_{s2}(t) + c_s\dot{y}_{s2}(t) + k_{s2}y_{s2}(t) = 0, \quad s = 1, 2, \ldots, N. \tag{21}$$

Eqs. (20) and (21) are valid only when the sth vehicle acts on the bridge.

Eqs. (18), (20) and (21) can be written together in matrix form as

$$\begin{bmatrix} \mathbf{M} & \mathbf{\Phi M}_1 & \mathbf{\Phi M}_2 \\ \mathbf{0} & \mathbf{M}_1 & \mathbf{0} \\ \mathbf{0} & \mathbf{0} & \mathbf{M}_2 \end{bmatrix} \begin{Bmatrix} \ddot{\mathbf{q}} \\ \ddot{\mathbf{y}}_1 \\ \ddot{\mathbf{y}}_2 \end{Bmatrix} + \begin{bmatrix} \mathbf{0} & \mathbf{0} & \mathbf{0} \\ \mathbf{0} & \mathbf{C} & -\mathbf{C} \\ \mathbf{0} & -\mathbf{C} & \mathbf{C} \end{bmatrix} \begin{Bmatrix} \dot{\mathbf{q}} \\ \dot{\mathbf{y}}_1 \\ \dot{\mathbf{y}}_2 \end{Bmatrix}$$
$$+ \begin{bmatrix} \mathbf{K} & \mathbf{0} & \mathbf{0} \\ -\mathbf{K}_1\mathbf{\Phi}^{\mathrm{T}} & \mathbf{K}_1 + \mathbf{K}_2 & -\mathbf{K}_2 \\ \mathbf{0} & -\mathbf{K}_2 & \mathbf{K}_2 \end{bmatrix} \begin{Bmatrix} \mathbf{q} \\ \mathbf{y}_1 \\ \mathbf{y}_2 \end{Bmatrix} = \begin{Bmatrix} \mathbf{p} \\ \mathbf{K}_1\mathbf{r} \\ \mathbf{0} \end{Bmatrix}, \tag{22}$$

where the sub-matrices and sub-vectors are given below:

$$\mathbf{M} = [m_{ij}], \quad \mathbf{K} = [k_{ij}], \quad i, j = 1, 2, \ldots, n, \tag{23–24}$$

$$\mathbf{\Phi} = [\phi_i(x_s(t))], \quad i = 1, 2, \ldots, n; \ s = 1, 2, \ldots, N, \tag{25}$$

$$\mathbf{M}_1 = \mathrm{diag}[M_{s1}], \quad \mathbf{M}_2 = \mathrm{diag}[M_{s2}], \quad \mathbf{C} = \mathrm{diag}[c_s], \quad s = 1, 2, \ldots, N, \tag{26–28}$$

$$\mathbf{K}_1 = \mathrm{diag}[k_{s1}], \quad \mathbf{K}_2 = \mathrm{diag}[k_{s2}], \quad s = 1, 2, \ldots, N, \tag{29–30}$$

$$\mathbf{y}_1 = \{y_{s1}(t)\}^{\mathrm{T}}, \quad \mathbf{y}_2 = \{y_{s2}(t)\}^{\mathrm{T}}, \quad \mathbf{r} = \{r(x_s(t)\}^{\mathrm{T}}, \quad s = 1, 2, \ldots, N, \tag{31–33}$$

$$\mathbf{p} = \{p_i(t)\}^{\mathrm{T}}, \quad \mathbf{q} = \{q_i(t)\}^{\mathrm{T}}, \quad i = 1, 2, \ldots, n. \tag{34–35}$$

Eq. (22) can be solved by the Newmark-β method or similar. Then $\{q_i(t)\}$ and $\{\ddot{q}_i(t)\}$ are obtained accordingly. The simulated "noise-free" acceleration time history $a_{nf}(x, t)$ of the bridge at measurement location x can then be expressed as

$$a_{nf}(x, t) = \ddot{y}(x, t) = \sum_{i=1}^{n} \ddot{q}_i(t)\,\phi_i(x). \tag{36}$$

The vector containing the simulated "noise-free" acceleration time histories at the measurement stations then forms the noise-free acceleration vector $\mathbf{A}_{nf}$.

In the study, the random road surface roughness $r(x)$ of the bridge is described by a kind of zero-mean, real-valued, stationary Gaussian process [20] as

$$r(x) = \sum_{h=1}^{N_T} \alpha_h \cos(2\pi\omega_h x + \Phi_h), \tag{37}$$

where the roughness parameter α_h is the amplitude of the cosine wave, Φ_h is a random phase angle with uniform probability distribution in the interval $[0, 2\pi]$, ω_h is a frequency within the interval $[\omega_l, \omega_u]$ in which the power spectral density function $S_r(\omega_h)$ (in m^3/cycle) is defined, x is the position measured from the left end of the bridge and N_T is the total number of terms used to build up the road surface roughness. The parameters α_h and ω_h are computed, respectively, by

$$\alpha_h^2 = 4S_r(\omega_h)\Delta\omega, \tag{38}$$

$$\omega_h = \omega_l + (h - 1/2)\Delta\omega, \quad h = 1, 2, \ldots, N_T, \tag{39}$$

$$\Delta\omega = (\omega_u - \omega_l)/N_T, \tag{40}$$

in which ω_l and ω_u are the lower and upper cut-off spatial frequencies (in cycles/m) respectively. The power spectral density function $S_r(\omega_h)$ can be expressed in terms of the spatial frequency ω_h of the road surface roughness as

$$S_r(\omega_h) = \begin{cases} \bar{\alpha}\omega_h^{-\beta} & \text{for } \omega_l < \omega_h < \omega_u, \\ 0 & \text{elsewhere,} \end{cases} \tag{41}$$

where $\bar{\alpha}$ is a spectral roughness coefficient in m^2/(m/cycle) and the exponent β is taken to be 1.94 [20]. The value of $\bar{\alpha}$ is determined based on the classification of road surface condition according to ISO specification [21].

2.3. Simulation of measurement noise

Real life measurements are usually polluted by noise. To evaluate the sensitivity of results to such measurement noise, noise-polluted measurements are simulated by adding to the noise-free acceleration vector a corresponding noise vector whose root-mean-square (r.m.s.) value is equal to a certain percentage of the r.m.s. value of the noise-free data vector. The components of all the noise vectors are of Gaussian distribution, uncorrelated and with a zero mean and unit standard deviation. Then on the basis of the noise-free acceleration $\mathbf{A}_{nf}$, the noise-polluted acceleration $\mathbf{A}_{np}$ of the bridge at location x can be simulated by

$$\mathbf{A}_{np} = \mathbf{A}_{nf} + RMS(\mathbf{A}_{nf}) \cdot N_{level} \cdot \mathbf{N}_{unit}, \tag{42}$$

where $RMS(\mathbf{A}_{nf})$ is the r.m.s. value of the noise-free acceleration vector $\mathbf{A}_{nf}$, N_{level} is the noise level, and $\mathbf{N}_{unit}$ is a randomly generated noise vector with zero mean and unit standard deviation. In the present study, besides the case of zero noise, three levels of noise pollution will be investigated, namely 1%, 5% and 10%.

3. Multi-stage identification based on genetic algorithms

3.1. Application of genetic algorithms

In the present identification problem, the errors at the measurement stations between the measured accelerations and the reconstructed accelerations from the identified parameters should be minimized. For a bridge with Q measurement stations and a total of R time points in each

measured time history, the objective function F to be maximized in the present study can be written in terms of the error vector $\mathbf{e}_i$ as

$$F = -\sum_{i=1}^{Q} \|\mathbf{e}_i\|_2 = -\sum_{i=1}^{Q}\left(\sum_{j=1}^{R} (e_{ij})^2\right)^{1/2}, \tag{43}$$

where $\|\mathbf{e}_i\|_2$ is the Euclidean vector norm of the error vector $\mathbf{e}_i$ that is defined as

$$\mathbf{e}_i = \{a_{ij,simu}\} - \{a_{ij,iden}\}. \tag{44}$$

$a_{ij,simu}$ is the element of the simulated acceleration vector and $a_{ij,iden}$ is the element of the acceleration vector calculated from the trial vehicle parameters in each generation, both at the ith measurement station and the jth time point. The identification is realized through a robust multi-stage optimization scheme based on genetic algorithms. Starting from the very wide initial variable domains, this multi-stage optimization scheme reduces the variable search domains stage by stage using the identified results of the previous stage.

Genetic algorithms [18,19] are stochastic global search techniques based on the mechanics of natural selection and natural genetics. They combine survival of the fittest among string structures with a structured yet randomized information exchange to form a search algorithm with some of the innovative flair of human search. The search and optimization direction of genetic algorithms is definitely guided to global optimal values of the variables.

In the present study, the main variables to be identified are the vehicle parameters, namely, the equivalent lower and upper masses, the damping coefficient, the contact stiffness and the primary stiffness for each vehicle. Because of the uncertainty of the real road surface roughness, it is impractical to identify the roughness itself directly. Again using the spectral approach, Eq. (37) is adopted to build up the roughness approximately using the parameters of a few terms, namely, the amplitude of the cosine wave α_h, the phase angle Φ_h, and the roughness frequency ω_h. Assuming that there are all together N vehicles on a bridge and the roughness is built up using N_T terms, the number of parameters to be identified is therefore $(5N + 3N_T)$. All the parameters are coded as binary strings, which are assembled together to form an individual in the optimization using genetic algorithms. Techniques similar to a previous study [17] are adopted, including the use of linear fitness scaling [18] to ensure competition and the mapping to enforce that the raw fitness f is always positive. The randomized techniques of genetic algorithms work very well on this identification problem.

3.2. Multi-stage optimization

To kick off the search and optimization process, a selected number of individuals are randomly created to form an initial population in the beginning of the process. In the present parameter identification problem, an obvious and exact search domain is always difficult to find. Although the identification of the contact forces provides useful clues to the identification of moving masses [16], this may not be as useful here as much more parameters are involved in the present 5-parameter vehicle model and some of the parameters are not directly related to the force of gravity. In order not to miss the global optimal set of parameters and converge on a wrong solution, the initial search domain for each variable must be set sufficiently large. However within

these very large search domains, it is often difficult to find the ideal global optimal values by a single optimization run, and it also takes an extremely long running time. In order to overcome this problem, the parameter identification is carried out through a multi-stage optimization scheme involving the repeated use of genetic algorithms and gradual refinement of search domains as well as accuracy. Using reasonable string lengths and a relatively small number of generations, it is possible for the initial stage of optimization to produce rough estimates of the parameters. Such estimates are then used to map out the refined search domains for the second stage. It is known that the genetic optimization gradually guides the trial solutions to the optimal one. Therefore through this staged optimization process, the search domains will be reducing in each successive stage in the light of the identification results of the previous stage.

In the present study, all vehicle parameters to be identified are non-negative values, and so the lower limits of their initial search domains are all set as zero. The upper limits of the initial search domains for the spring stiffnesses and the damping coefficient are set large enough. For both the lower and upper masses for normal bridges, a convenient upper limit of the initial search domain can be determined in the light of available information of common vehicles. As for the roughness parameters, the phase angle Φ_h should be located within $[0, 2\pi]$ based on its definition, while the search domains for the cosine wave amplitude α_h and the roughness frequency ω_h can be estimated from the road surface conditions and practical experience. These search domains can then be narrowed down in subsequent stages of optimization. For example, assuming the identified lower mass of the sth vehicle in a stage to be $M_{s1,iden}$, the search domain D of this mass for the next stage can be set as

$$D = (D_l, D_u) = M_{s1,iden}(C_l, C_u), \quad 0 < C_l < 1; \quad 1 < C_u, \tag{45}$$

where C_l and C_u are, respectively, coefficients to define the lower limit D_l and the upper limit D_u of the search domain D. The same strategy can be applied to the other parameters. The values of C_l and C_u may be varied at different stages for improved efficiency. As different parameters converge at different rates, the values of C_l and C_u may also be controlled suitably bearing in mind efficiency and the relative likelihood of the correct values. The termination of the search at each stage is controlled both by the maximum number of generations as well as the changes of parameters between successive generations. The termination of the whole procedure is controlled by the difference between the parameters identified from two adjacent stages.

4. Numerical simulations

4.1. General description

To evaluate the efficiency of the proposed method, a series of comprehensive case studies covering various aspects have been carried out. Apart from the comparison of the present 5-parameter vehicle model and the former 4-parameter vehicle model [17], the effects of number of measurement stations, levels of measurement noise, and number of vehicles on the accuracy are also examined. The contact forces between the moving vehicles and the bridge surface are also estimated using the identified vehicle parameters. The identification error $Error_{iden}$ of, for

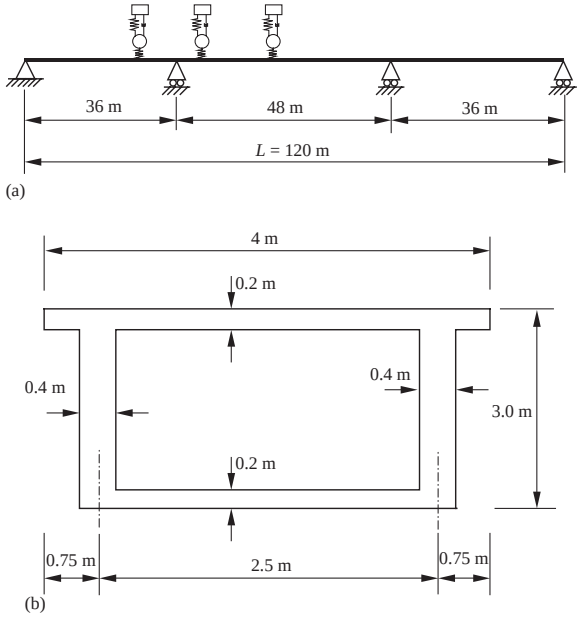

Fig. 2. A three-span continuous bridge: (a) idealized beam model; (b) idealized cross-section.

example, the lower mass of sth vehicle is defined as

$$Error_{iden} = \frac{|M_{s1,iden} - M_{s1,true}|}{M_{s1,true}} \times 100\%, \tag{46}$$

where $M_{s1,iden}$ and $M_{s1,true}$ are the identified and true values of the lower mass M_{s1} respectively. Definitions for the other parameters are similar.

A three-span continuous box girder bridge is used in the case studies, and the idealized beam model and cross-section are shown in Fig. 2. The density ρ and Young's modulus E of concrete are 2400 kg/m^3 and 30 000 MPa respectively. The span lengths from left to right are 36, 48, 36 m respectively. The cross-sectional area A and the second moment of inertia I are 3.46 m^2 and 3.854 m^4 respectively. The dynamic behaviour of a bridge is primarily governed by the first few vibration modes. For both the acceleration simulation and parameter identification, the first three vibration modes of the bridge are adopted as a compromise. All the vehicles are assumed to travel at a horizontal speed v of 17 m/s across the bridge, as this is a normal speed on highways. The distance between adjacent vehicles is 10.0 m. The total traversing time T, which is counted from the instant when the first vehicle arrives at the starting end of the bridge to that when the last vehicle leaves the bridge, is divided into 200 time intervals. The histories of acceleration and contact forces are therefore presented accordingly with respect to the time ratio t/T.

Only one vehicle is considered in Case Studies 1–4, and the assumed vehicle parameters used to simulate the accelerations are those of Vehicle 1 in Table 1. In Case Study 5, a 3-vehicle convoy is studied, and the corresponding assumed parameters are shown in Table 1. The road surface condition is assumed to be good in all case studies, having a spectral roughness coefficient $\bar{\alpha}$ of 0.6×10^{-6} m^2/(m/cycle), with lower and upper cut-off spatial frequencies $\omega_l = 0.1$ cycles/m and

Table 1
Assumed true vehicle parameters

Vehicle	Lower mass M_{s1} (kg)	Upper mass M_{s2} (kg)	Damping coefficient c (Ns/m)	Contact spring stiffness k_{s1} (N/m)	Primary spring stiffness k_{s2} (N/m)	Case Study
1	4800	27 000	86 000	500 000	9.12×10^6	1–5
2	3600	21 000	60 000	400 000	8.68×10^6	5
3	6000	36 000	100 000	600 000	10.0×10^6	5

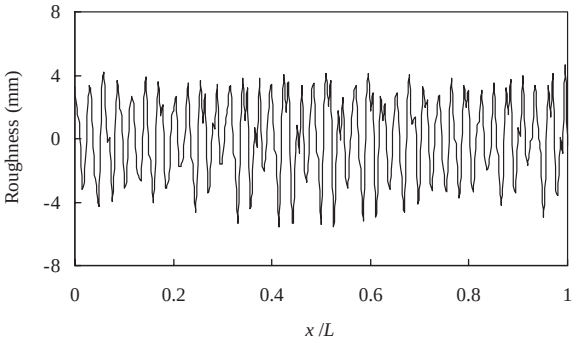

Fig. 3. A typical bridge road surface roughness profile adopted in present study.

$\omega_u = 4.0$ cycles/m respectively. Using Eqs. (37)–(41) and a total of 10 terms (i.e. $N_T = 10$), the random road surface roughness profile as shown in Fig. 3 is generated for acceleration simulation. The simulated road surface roughness ranges from 6.0 to -6.0 mm, which is reasonable for a real bridge with good road surface condition. Case Study 4 examines the effect of measurement noise, while the other case studies focusing on other aspects make use of noise-free simulated signals.

For the purpose of identification, the initial search domains of the vehicle parameters for every vehicle are assumed to be $M_1 \in (0, 10\,000)$ kg, $M_2 \in (0, 60\,000)$ kg, $c \in (0, 200\,000)$ Ns/m, $k_1 \in (0, 10^7)$ N/m and $k_2 \in (0, 2 \times 10^8)$ N/m. The initial search domains of the three kinds of roughness parameters are set as $\alpha_h \in (-10, 10)$ mm, $\Phi_h \in [0, 2\pi]$, and $\omega_h \in (0.01, 10.0)$ cycles/m. To be practical, only four terms for modelling the roughness have been used in the identification process. Therefore for the cases involving one and three vehicles, the total numbers of the parameters to be identified are 17 and 27 respectively. Unless otherwise stated, the population size used in the case studies is set as 150 in each generation and the number of generations in each stage is 300. The parameters for the present genetic algorithm with uniform crossover [17] are as follows: crossover probability $P_c = 0.5$, creep mutation probability $P_{cm} = 0.04$, and jump mutation probability $P_{jm} = 1/N_{pop}$, where N_{pop} denotes the population size.

4.2. Case Study 1: effect of vehicle models

The choice of the vehicle model in the solution of a vehicle–bridge interaction problem is especially important when the road surface roughness is taken into account. As opposed to

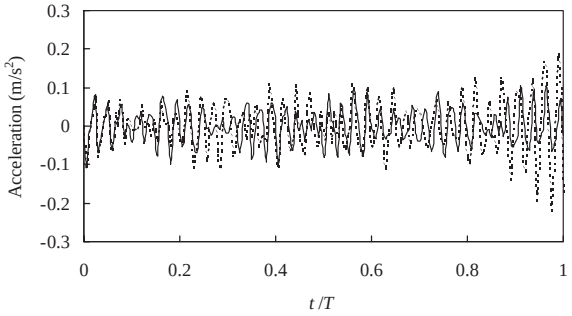

Fig. 4. Dynamic accelerations at location $x = 12.0$ m on the bridge under a 5-parameter vehicle with $k_1 = 5.0 \times 10^5$ N/m; ——, roughness neglected; - - - -, roughness considered.

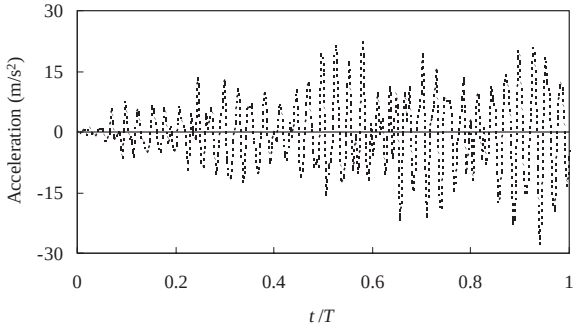

Fig. 5. Dynamic accelerations at location $x = 12.0$ m on the bridge under a 4-parameter vehicle; ——, roughness neglected; - - - -, roughness considered.

railway vehicles having very stiff wheels, highway vehicles normally have tyres with comparatively lower stiffness. In this study, a comparison is made between the present 5-parameter vehicle model and the former 4-parameter vehicle model [17] on their ability to cope with road surface roughness. Here only one vehicle is considered.

The acceleration histories at location $x = 12$ m on the bridge obtained using the present 5-parameter vehicle with and without roughness are shown in Fig. 4. Using the 5-parameter vehicle model having reasonable parameters, the difference between the two acceleration histories is noticeable but their orders of magnitude are comparable, which is close to the real situation as the road surface condition is assumed to be good. Omitting the tyre contact stiffness k_{s1}, the 5-parameter vehicle model degenerates into a 4-parameter vehicle model. The acceleration histories obtained at the same location using the degenerated 4-parameter vehicle model with and without roughness are shown in Fig. 5. It can be seen that, without considering the tyre contact stiffness, the impact effect has been grossly over-amplified and the 4-parameter vehicle model may easily predict separation between the vehicle and the bridge [22].

4.3. Case Study 2: basic strategy

This case study is mainly to establish the validity and effectiveness of the proposed multi-stage optimization procedure. There is only one moving vehicle with simulated noise-free accelerations at six measurement stations along the bridge, namely at $x_1 = 12$ m, $x_2 = 24$ m, $x_3 = 52$ m, $x_4 = 68$ m, $x_5 = 96$ m, and $x_6 = 108$ m. Table 2 shows the parameters identified in the three stages of optimization. It is observed that the estimates for the masses have swiftly come close to the true values after the first stage, whereas the other parameters need more computations to converge and their final values are also less accurate than the mass values. The search domains at a new stage of optimization are mapped out using Eq. (45) based on the identified values in the previous stage. The time histories of contact force calculated from the true and identified vehicle parameters are shown in Fig. 6. The trends of the time histories are mainly governed by the masses, and they tend

Table 2
The identification results of the first three stages in Case Study 2

Stage No.		Vehicle parameters				
		M_1 (kg)	M_2 (kg)	c (Ns/m)	k_1 (N/m)	k_2 (N/m)
1	Lower limit	0	0	0	0	0
	Upper limit	10 000	60 000	200 000	10×10^6	200×10^6
	Identified	4855	26 832	34 539	245 984	6 760 000
2	Lower limit	4370	24 100	10 400	73.8×10^3	3.38×10^6
	Upper limit	5340	29 500	104 000	738×10^3	13.5×10^6
	Identified	4855	26 832	68 737	478 352	6 760 000
3	Lower limit	4610	25 500	34 400	239×10^3	5.07×10^6
	Upper limit	5100	28 200	103 000	718×10^3	10.1×10^6
	Identified	4826	26 909	75 354	560 630	9 939 419
True values		4800	27 000	86 000	500 000	9 120 000
Identification errors (%)		0.54	0.34	12.38	12.13	8.98

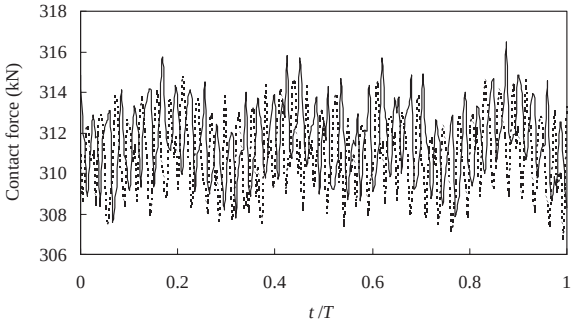

Fig. 6. Contact forces calculated from true and identified vehicle parameters in Case Study 2; true ——; identified - - - -.

Table 3
Arrangement of measurement stations in Case Study 3

Number of measurement stations	Distances of measurement stations from the left end (m)
3	18.0, 60.0, 102.0
6	12.0, 24.0, 52.0, 68.0, 96.0, 108.0
9	9.0, 18.0, 27.0, 48.0, 60.0, 72.0, 93.0, 102.0, 111.0
12	7.2, 14.4, 21.6, 28.2, 45.6, 55.2, 64.8, 74.4, 91.2, 98.4, 105.6, 112.8
15	6.0, 12.0, 18.0, 24.0, 30.0, 44.0, 52.0, 60.0, 68.0, 76.0, 90.0, 96.0, 102.0, 108.0

to agree well with each other, as their estimates are accurate. The discrepancies in contact force are mainly due to the slightly higher errors in the estimates of the spring stiffnesses and the damping coefficient. Even so, the overall trends of fluctuations of contact forces also agree well with each other.

4.4. Case Study 3: effect of number of measurement stations

Although a former study [17] shows that even one measurement station is often sufficient for identification, very often more than one accelerometer is used in field measurements. It not only improves the accuracy in most cases, but also caters for the possibility of occasional breakdown of certain instruments. The case of an increased number of measurement stations is studied here. For comparison, the identification problem is repeated using five patterns of up to 15 measurement stations, as summarized in Table 3. Only one vehicle is considered. The identification results of the five patterns of measurement stations after three stages of optimization are shown in Table 4. The time histories of contact force calculated from the true and the identified parameters from the arrangement comprising 3 measurement stations are plotted in Fig. 7. The corresponding results obtained from 15 measurement stations as shown in Fig. 8 indicate much better agreement with the reference time history.

Table 4 shows that starting from the same search domains, with the same genetic parameters and after the same number of optimization stages, using more measurement stations improves the accuracy but this is achieved at the expense of computation time. In other words, to aim at the same accuracy, the use of more measurement stations reduces the amount of subsequent computations. For the present three-span continuous bridge, the use of six measurement stations may be taken as a compromise in view of the amount of field measurements, the computation time and the accuracy of results.

4.5. Case Study 4: effect of measurement noise

To investigate the effect of measurement noise on the accuracy and efficiency of the proposed method, three levels of measurement noise are considered in this case study, namely 1%, 5% and 10%. Apart from the presence of measurement noise, all the rest are identical to those in Case Study 2. At least three stages of optimization are carried out and the decision to go further is based on the differences between parameters identified in successive stages. Table 5 shows the final

Table 4
Effects of number of measurement stations in Case Study 3

Number of measurement stations	Identified values					Identification errors				
	M_1 (kg)	M_2 (kg)	c (N s/m)	k_1 (N/m)	k_2 (N/m)	M_1 (%)	M_2 (%)	c (%)	k_1 (%)	k_2 (%)
3	4745	27 126	68 478	583 258	7 617 032	1.15	0.47	20.29	16.65	16.48
6	4826	26 909	75 354	560 630	9 939 419	0.54	0.34	12.38	12.13	8.98
9	4782	27 087	78 573	535 762	9 813 123	0.38	0.32	8.64	7.15	7.60
12	4818	26 928	91 974	472 834	8 593 776	0.38	0.27	6.95	5.43	5.77
15	4786	27 012	80 986	484 209	9 466 355	0.29	0.04	5.83	3.15	3.80

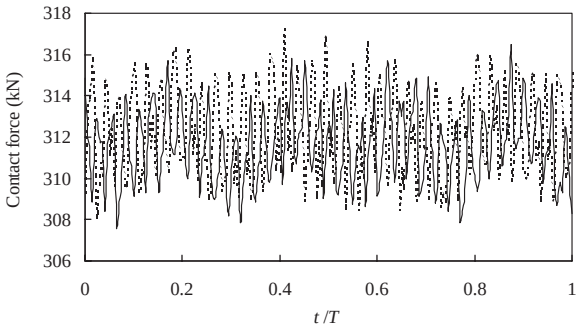

Fig. 7. Contact forces calculated from true and identified vehicle parameters in Case Study 3 for the arrangement comprising three measurement stations; true ——; identified - - - -.

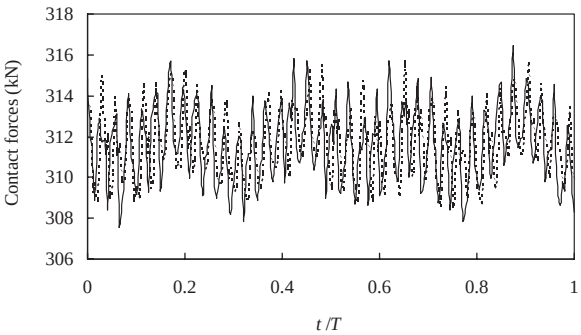

Fig. 8. Contact forces calculated from true and identified vehicle parameters in Case Study 3 for the arrangement comprising 15 measurement stations; true ——; identified - - - -.

results for three different levels of measurement noise compared with those without noise. The time histories of contact forces calculated from the true and the identified parameters for the case of 10% measurement noise are shown in Fig. 9.

Table 5
Effect of measurement noise in Case Study 4

Noise level	No. of stages	Identified values					Identification errors				
		M_1 (kg)	M_2 (kg)	c (N s/m)	k_1 (N/m)	k_2 (N/m)	M_1 (%)	M_2 (%)	c (%)	k_1 (%)	k_2 (%)
0%	3	4826	26 909	75 354	560 630	9 939 419	0.54	0.34	12.4	12.1	8.98
1%	3	4774	27 091	73 685	569 296	9 978 512	0.55	0.34	14.3	13.9	9.41
5%	4	4830	26 902	71 767	429 150	8 180 640	0.63	0.36	16.6	14.2	10.3
10%	5	4768	27 130	101 936	573 356	7 952 642	0.67	0.48	18.5	14.7	12.8

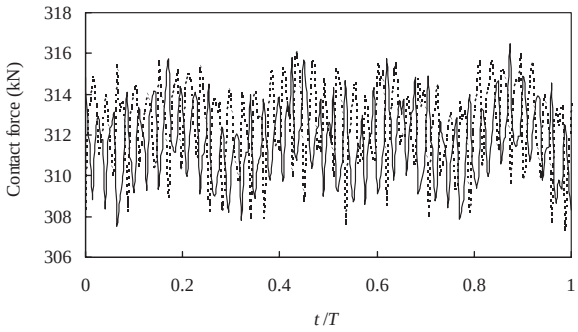

Fig. 9. Contact forces calculated from true and identified vehicle parameters in Case Study 4; true ——; identified - - - -.

It is seen from Table 5 that the identification results do not vary much with the increase in the measurement noise level. This demonstrates that the proposed identification procedure is not particularly sensitive to reasonable measurement noise. However the more measurement noise there is, the more optimization stages are required.

4.6. Case Study 5: effect of number of moving vehicles

In real life, there are always many vehicles on a bridge at the same time. In order to test the accuracy and efficiency of the proposed method for more practical situations, a convoy comprising three vehicles at a spacing of 10 m is therefore considered and their true parameters are shown in Table 1. The same arrangement of six measurement stations as in Case Study 2 is also used here. In view of the relatively large number of parameters to be identified in this case, the population size is set as 300. The number of genetic generations in each stage is taken as 150. The identification results after the first three stages are shown in Table 6.

The identification results in Table 6 are very acceptable, which means that the proposed optimization procedure produces acceptable identification results for a multi-vehicle convoy similar to the case of only one vehicle. In addition, the optimization speed and computation time are also similar.

Table 6
Effect of number of moving vehicles in Case Study 5

Vehicle	Identified values					Identification errors				
	M_1 (kg)	M_2 (kg)	c (N s/m)	k_1 (N/m)	k_2 (N/m)	M_1 (%)	M_2 (%)	c (%)	k_1 (%)	k_2 (%)
1	4784	27 063	97 636	547 993	8 314 704	0.33	0.23	13.53	9.60	8.83
2	3608	20 927	67 472	448 041	7 843 248	0.22	0.35	12.45	12.01	9.64
3	5979	36 108	115 833	668 937	9 176 031	0.35	0.30	15.83	11.49	8.24

4.7. Discussions

Case Study 1 shows that the present 5-parameter vehicle model is a more reasonable choice to be used for dynamic analysis and identification when the road surface roughness is taken into account. Case Study 2 validates the present multi-stage identification procedure. In the other cases, the proposed procedure is examined on various aspects including the effects of number of measurement stations, noise level of acceleration measurements, and number of vehicles. The results confirm that this identification method is very robust. When the road surface roughness is considered together with a reasonably measurement noise level, very acceptable results can be obtained even for a multi-vehicle convoy after only a few optimization stages with an appropriate population size. A relatively small number of measurement stations are sufficient for the proposed identification process, which saves much computation time. Examination of all the identification results of the case studies above shows that the identification errors of the two spring stiffness values and the damping coefficient are comparatively larger than those of the two masses.

5. Conclusions

A procedure for parameter identification of vehicles moving on multi-span continuous bridges taking into account road surface roughness is described. The proposed moving vehicle model comprises lower and upper masses interconnected by a damper and a primary spring, with another spring to model the contact stiffness between the tyres and the bridge deck. The aim of the study is to identify the associated vehicle parameters based on the acceleration measurements at selected stations. Here the acceleration measurements are simulated by the numerical solution to the associated forward problem taking into consideration random road surface roughness, with random measurement noise introduced subsequently to account for the likely errors in practice. The search for the vehicle parameters is formulated as an optimization problem in which the error between the measured accelerations and the accelerations reconstructed from trial parameters is minimized. A robust multi-stage optimization scheme based on genetic algorithms has been proposed in which the search domains are systematically reduced stage by stage. The optimal solution is achieved within the re-defined search domains. A series of comprehensive case studies have been carried out to test the proposed model and procedure. It shows that the present 5-parameter vehicle model is a favourable choice to be used for identification. In spite of the

presence of measurement noise and uncertain road surface irregularity, acceptable results are obtained for a solitary vehicle or a convoy.

Acknowledgements

The work described in this paper has been partially supported by the Committee on Research and Conference Grants, The University of Hong Kong, Hong Kong, China. The present study has made use of the code of a genetic algorithm written by Dr. D.L. Carroll at University of Illinois, and this is gratefully acknowledged.

References

[1] A. Soom, J.W. Chen, Simulation of random surface roughness-induced contact vibrations at Hertzian contacts during steady sliding, *Journal of Tribology, Transactions of the American Society of Mechanical Engineers* 108 (1) (1986) 123–127.
[2] P. Remington, J.D. Stahr, Effects on noise of changes in wheel/rail system parameters, *Journal of Sound and Vibration* 87 (2) (1981) 221–229.
[3] P. Remington, Control of wheel/rail rolling noise at the source, *Heavy Vehicle Systems* 7 (1) (2000) 1–21.
[4] P. Remington, J. Webb, Wheel/rail noise reduction through profile modification, *Journal of Sound and Vibration* 193 (1) (1996) 335–348.
[5] Y. Zhang, C. Hazard, Effects of tire properties and their interaction with the ground and suspension on vehicle dynamic behaviour—a finite element approach, *Tire Science and Technology* 27 (4) (1999) 227–249.
[6] B.I. Bachrach, Pneumatic damping of vehicle tires to improve ride quality, *Proceedings—Society of Automotive Engineers, the 5th International Conference on Vehicular Structural Mechanics*, Detroit, Michigan, USA, 1984, pp. 229–235.
[7] A.P. Whittemore, Measurement and prediction of dynamic pavement loading by heavy highway vehicles, SAE-Paper 690524, 1969, 5p.
[8] M. El-Gindy, L. Ilosvai, Computer simulation study on a vehicle's directional response in some severe manoeuvres. Part 1: rapid lane-change manoeuvres, *International Journal of Vehicle Design* 4 (4) (1983) 386–401.
[9] R.K. Taylor, L.L. Bashford, M.D. Schrock, Methods for measuring vertical tire stiffness, *Transactions of the American Society of Agricultural Engineers* 43 (6) (2000) 1415–1419.
[10] R.K. Sleeper, R.C. Dreher, Tire stiffness and damping determined from static and free-vibration tests, NASA Technical Paper 1671, 1980, 45p.
[11] F.T.K. Au, Y.S. Cheng, Y.K. Cheung, Effects of random road surface roughness and long-term deflection of prestressed concrete girder and cable-stayed bridges on impact due to moving vehicles, *Computers and Structures* 79 (2001) 853–872.
[12] Y. Ryu, Y. Terumichi, Y. Suda, S. Ohno, Coupled vibration analysis model of a wheel/railway track system with consideration of the contact stiffness, *Transactions of the Japan Society of Mechanical Engineers, Part C* 62 (603) (1996) 4147–4152.
[13] S.G. Hutton, Y.K. Cheung, Dynamic response of single span highway bridges, *Earthquake Engineering & Structural Dynamics* 7 (6) (1979) 543–553.
[14] D.Y. Zheng, Y.K. Cheung, F.T.K. Au, Y.S. Cheng, Vibration of multi-span non-uniform beams under moving loads by using modified beam vibration functions, *Journal of Sound and Vibration* 212 (3) (1998) 455–467.
[15] X.Q. Zhu, S.S. Law, Moving forces identification on a multi-span continuous bridge, *Journal of Sound and Vibration* 228 (2) (1999) 377–396.
[16] R.J. Jiang, F.T.K. Au, Y.K. Cheung, Identification of masses moving on multi-span beams based on a genetic algorithm, *Computers & Structures* 81 (2003) 2137–2148.

[17] F.T.K. Au, R.J. Jiang, Y.K. Cheung, Parameter identification of vehicles moving on continuous bridges, *Journal of Sound and Vibration* 269 (1–2) (2004) 91–111.
[18] D.E. Goldberg, *Genetic Algorithms in Search, Optimization, and Machine Learning*, Addison-Wesley Publishing Company, Inc., Reading, MA, USA, 1989.
[19] M. Gen, R. Cheng, *Genetic Algorithms & Engineering Optimization*, Wiley, New York, USA, 2000.
[20] H. Honda, Y. Kajikawa, T. Kobori, Spectra of road surface roughness on bridges, *Journal of the Structural Division* 108 (ST9) (1982) 1956–1966.
[21] International Organization for Standardization, ISO/TC 108/WG9, BSI proposals for generalized road inputs to vehicles, Document No. 5, 1972.
[22] Y.S. Cheng, F.T.K. Au, Y.K. Cheung, D.Y. Zheng, On the separation between moving vehicles and bridge, *Journal of Sound and Vibration* 222 (5) (1999) 781–801.